

# Effect of $\text{Fe}^{2+}$ on garnet–melt trace element partitioning: experiments in FCMAS and quantification of crystal-chemical controls in natural systems

Wim van Westrenen\*, Jonathan D. Blundy, Bernard J. Wood

*CETSEI, Department of Earth Sciences, University of Bristol, Wills Memorial Building, Queen's Road, Bristol BS8 1RJ, UK*

---

## Abstract

Garnet–melt trace element partitioning experiments were performed in the system  $\text{FeO–CaO–MgO–Al}_2\text{O}_3\text{–SiO}_2$  (FCMAS) at 3 GPa and 1540°C, aimed specifically at studying the effect of garnet  $\text{Fe}^{2+}$  content on partition coefficients ( $D^{\text{Grt}/\text{Melt}}$ ).  $D^{\text{Grt}/\text{Melt}}$ , measured by SIMS, for trivalent elements entering the garnet X-site show a small but significant dependence on garnet almandine content. This dependence is rationalised using the lattice strain model of Blundy and Wood [Blundy, J.D., Wood, B.J., 1994. Prediction of crystal–melt partition coefficients from elastic moduli. *Nature* 372, 452–454], which describes partitioning of an element  $i$  with radius  $r_i$  and valency  $Z$  in terms of three parameters: the effective radius of the site  $r_0(Z)$ , the strain-free partition coefficient  $D_0(Z)$  for a cation with radius  $r_0(Z)$ , and the apparent compressibility of the garnet X-site given by its Young's modulus  $E_X(Z)$ . Combination of these results with data in Fe-free systems [Van Westrenen, W., Blundy, J.D., Wood, B.J., 1999. Crystal-chemical controls on trace element partitioning between garnet and anhydrous silicate melt. *Am. Mineral.* 84, 838–847] and crystal structure data for spessartine, andradite, and uvarovite, leads to the following equations for  $r_0(3+)$  and  $E_X(3+)$  as a function of garnet composition ( $X$ ) and pressure ( $P$ ):

$$r_0(3+) [\text{\AA}] = 0.930 X_{\text{Py}} + 0.993 X_{\text{Gr}} + 0.916 X_{\text{Alm}} + 0.946 X_{\text{Spes}} + 1.05 (X_{\text{And}} + X_{\text{Uv}}) - 0.005 (P [\text{GPa}] - 3.0) (\pm 0.005 \text{\AA})$$

$$E_X(3+) [\text{GPa}] = 3.5 \times 10^{12} (1.38 + r_0(3+) [\text{\AA}])^{-26.7} (\pm 30 \text{GPa})$$

Accuracy of these equations is shown by application to the existing garnet–melt partitioning database, covering a wide range of  $P$  and  $T$  conditions ( $1.8 \text{ GPa} < P < 5.0 \text{ GPa}$ ;  $975^\circ\text{C} < T < 1640^\circ\text{C}$ ).  $D^{\text{Grt}/\text{Melt}}$  for all 3+ elements entering the X-site (REE, Sc and Y) are predicted to within 10–40% at given  $P$ ,  $T$ , and  $X$ , when  $D^{\text{Grt}/\text{Melt}}$  for just one of these elements is known. In the absence of such knowledge, relative element fractionation (e.g.  $D_{\text{Sm}}^{\text{Grt}/\text{Melt}}/D_{\text{Nd}}^{\text{Grt}/\text{Melt}}$ ) can be predicted. As an example, we predict that during partial melting of garnet peridotite, group A eclogite, and garnet pyroxenite,  $r_0(3+)$  for garnets ranges from  $0.939 \pm 0.005$  to  $0.953 \pm 0.009 \text{\AA}$ . These values are consistently smaller than the ionic radius of the

---

\* Corresponding author. Tel.: +44-117-954-5403; fax: +44-117-925-3385.  
E-mail address: w.van-westrenen@bristol.ac.uk (W. van Westrenen).

heaviest REE, Lu. The above equations quantify the crystal-chemical controls on garnet–melt partitioning for the REE, Y and Sc. As such, they represent a major advance en route to predicting  $D^{\text{Grt}/\text{Melt}}$  for these elements as a function of  $P$ ,  $T$  and  $X$ . © 2000 Elsevier Science B.V. All rights reserved.

**Keywords:** Experimental studies; Garnet group; Trace elements; Partitioning; Crystal chemistry

## 1. Introduction

Detailed knowledge about the partitioning of trace elements between mantle phases (especially clinopyroxene and garnet) and coexisting silicate melts is critically important for mantle melting studies. The current controversy over the presence of garnet in the source of basaltic magmas formed below mid-ocean ridges (MORB) provides a good example. MORB Sm–Nd and Lu–Hf systematics (e.g. Salters, 1996) and REE patterns (Shen and Forsyth, 1995) appear to require the presence of garnet in the MORB source. Observed U–Th disequilibrium in present-day MORB (e.g. Bourdon et al., 1996) requires a mineral phase somewhere in the MORB source which retains U preferentially over Th, inferred to be garnet from partitioning experiments (e.g. Beattie, 1993; LaTourrette et al., 1993; Hauri et al., 1994). Conversely, Blundy et al. (1998) and Wood et al. (1999), show that clinopyroxene can impose garnet-like signatures (i.e., compatibility of HREE and preferential retention of U over Th) on near-solidus mantle melts, possibly obviating the need for any garnet in the source of many MORB. Experimentally derived differences between garnet–melt and clinopyroxene–melt partition coefficients ( $D^{\text{Grt}/\text{Melt}}$  vs.  $D^{\text{Cpx}/\text{Melt}}$ ) therefore play a crucial role in arguments both in favour of and against a critical role for garnet. This example illustrates the importance of taking into account variations in  $D^{\text{Grt}/\text{Melt}}$  and  $D^{\text{Cpx}/\text{Melt}}$  with pressure ( $P$ ), temperature ( $T$ ), and bulk composition ( $X$ ). Although considerable progress has been made in predicting variations in  $D^{\text{Cpx}/\text{Melt}}$  (Wood and Blundy, 1997), to date no such model exists for garnet. This is particularly important in light of recent suggestions about the role of garnet pyroxenite veins in imposing the MORB ‘‘garnet signature’’ (e.g. Hirschmann and Stolper, 1996; Blichert-Toft et al., 1999). Partial melting of these veins would involve garnet–melt equilibria at pressures, temperatures, and in compositions, which are all very different from those used in published garnet–melt parti-

tioning experiments. There is therefore a need for a predictive garnet–melt partitioning model to fill these voids in the understanding of mantle melting.

In a previous paper (Van Westrenen et al., 1999) we quantified the crystal-chemical effects on garnet–anhydrous melt trace element partitioning along the pyrope–grossular join, for trivalent elements entering garnet X-sites (e.g. REE, Sc and Y). To extend our modelling to natural systems, well-constrained data on iron-bearing systems are needed. We therefore performed anhydrous experiments in the system FeO–CaO–MgO–Al<sub>2</sub>O<sub>3</sub>–SiO<sub>2</sub> (FCMAS), specifically aimed at isolating the effect of garnet iron content on partitioning. Results are interpreted within the framework of the Blundy and Wood (1994) model, which describes partitioning of an element  $i$  with radius  $r_i$  and valency  $Z$  in terms of three parameters: the effective radius of the site  $r_0$ , the strain-free partition coefficient  $D_0$  for a cation with radius  $r_0$ , and the apparent compressibility of the garnet X-site, given by its Young’s modulus  $E_X$ .

$$D_i^{\text{Grt}/\text{Melt}} = D_0^{\text{Grt}/\text{Melt}} \exp \left( \frac{-4\pi E_X N_A \left( \frac{r_0}{2} (r_i - r_0)^2 + \frac{1}{3} (r_i - r_0)^3 \right)}{RT} \right) \quad (1)$$

In Eq. (1),  $N_A$  is Avogadro’s number and  $R$  is the gas constant. Through combination with experiments in iron-free systems (Van Westrenen et al., 1999), we derive predictive equations for  $r_0(3+)$  and  $E_X(3+)$  as a function of garnet composition. These provide important constraints on partitioning in natural garnet–melt systems. To illustrate this, we use our model to predict that during mantle melting, Lu is the most compatible REE in garnet under all relevant  $P$ ,  $T$  and  $X$  conditions.

## 2. Experimental and analytical methods

Methods used for piston–cylinder experiments are identical to those described in Van Westrenen et al. (1999). After doping with appropriate amounts of 1000-ppm atomic absorption standard solutions, starting materials were dried at 110°C overnight, and then at 760°C for 10 min (prior to welding). Around 10 mg of the starting mix was placed in 2-mm O.D. graphite-lined Pt capsules, which were embedded in alumina and surrounded by a double sleeve of silica glass and BaCO<sub>3</sub>. A pressure correction of –13%, derived from Al-in-pyroxene barometry (Perkins et al., 1981), was applied to this configuration. Temperature was controlled to within 2°C by a W–3%Re/W–25%Re thermocouple, and the thermal gradient across the sample is less than 20°C. Starting materials were chosen to reproduce garnet–melt equilibria in FCMAS at 3.0 GPa (G. Gudfinnsson, unpublished data). Major element compositions of experimental products were determined with the University of Bristol JEOL 8600 electron microprobe, trace element levels (for Li, K, Sc, Ti, Sr, Y, Zr, Nb, La, Pr, Sm, Tb, Er, Yb, Lu, Hf, Ta, Re, U and Th) were measured with SIMS at the University of Edinburgh NSS Ion Probe Facility. Further details of starting mix preparation, analytical methods, their precision and accuracy can be found in Van Westrenen et al. (1999).

## 3. Results

Compositions of starting materials are given in Table 1. These compositions were determined from glasses prepared from aliquots of starting oxide mixtures, melted in air for 30 min, at 1520°C in unsealed Pt capsules. Concentrations of all trace elements were as expected from doping levels, with two exceptions: from the added amount of Re (520 ppm), only a small percentage (<4%, see Table 1) remained in the glass. This can be explained by the high volatility of Re at higher temperatures in air (J. Brenan, pers. comm.). Conversely, Sr concentrations were higher than expected from the doping level, as a result of unavoidable Sr contamination in the CaCO<sub>3</sub> used as a major component of our starting

Table 1

Major and trace element compositions of glassed starting materials

	A (low Fe)		B (high Fe)	
	Mean	$\sigma$	Mean	$\sigma$
FeO	4.5	0.1	17.2	0.3
CaO	12.4	0.1	9.50	0.1
MgO	19.7	0.2	14.6	0.1
Al <sub>2</sub> O <sub>3</sub>	16.6	0.1	10.8	0.1
SiO <sub>2</sub>	46.1	0.2	45.2	0.2
Total	99.2	0.3	97.3	0.4
<i>n</i>	20		38	
Li	39.1	0.8	38.5	0.6
K	898	13	1181	23
Sc	11.4	0.3	15.9	0.2
Ti	50.9	0.8	59.3	0.7
Sr	160	2	194	1
Y	8.79	0.10	11.1	0.1
Zr	22.0	2.4	23.6	1.6
Nb	38.5	1.0	50.1	0.7
La	162	2	48.2	0.6
Pr	13.8	0.1	16.3	0.2
Sm	9.43	0.26	13.0	0.4
Tb	9.12	0.14	11.1	0.2
Er	9.84	0.27	12.0	0.2
Yb	9.20	0.13	11.6	0.1
Lu	15.4	0.3	9.59	0.11
Hf	13.4	0.7	16.5	0.4
Ta	35.1	3.2	39.7	0.6
Re	6.86	0.54	15.6	2.7
Th	100	5	88.1	1.2
U	33.6	1.3	29.6	0.5
Total	1709		2216	
<i>n</i>	4		5	

Major elements in weight percent; trace elements in parts per million.

mix. Experimental conditions and products are given in Table 2. All experiments produced garnet, pyroxene and quench phase. Garnets were 40–100 μm in diameter, while pyroxenes were very small (generally <10 μm across). Major and trace element compositions of experimental products are given in Table 3. Pyroxene stoichiometries in experiments 16 and 18 are (Mg<sub>0.98</sub>Ca<sub>0.72</sub>Fe<sub>0.10</sub>Al<sub>0.19</sub>)(Si<sub>1.84</sub>Al<sub>0.16</sub>)O<sub>6</sub> and (Mg<sub>1.22</sub>Ca<sub>0.23</sub>Fe<sub>0.44</sub>Al<sub>0.11</sub>)(Si<sub>1.92</sub>Al<sub>0.08</sub>)O<sub>6</sub>. The CaO content of the latter is very low (5.8 wt.%), so this pyroxene could be described as an aluminous pigeonite. It is very close in composition to orthopyroxenes formed at virtually identical pressures and temperatures in a recent study of phase relationships

Table 2  
Experimental conditions and products

	16	18
Starting material	A	B
Capsules	C + Pt	C + Pt
<i>P</i> (GPa)	2.9	3.0
<i>T</i> (°C)	1540	1538
<i>t</i> (h)	21.5	21.5
Products	Grt (52) <sup>a</sup> Q (21) Px (27)	Grt (25) Q (65) Px (10)

<sup>a</sup>Proportions calculated from mass balance. Grt = garnet, Q = quenched melt, Px = pyroxene.

in lunar mare basalts (Longhi, 1992). Garnets have compositions Py<sub>72</sub>Gr<sub>19</sub>Alm<sub>9</sub> and Py<sub>56</sub>Gr<sub>13</sub>Alm<sub>31</sub>, re-

spectively, and no zoning was apparent in major elements. Garnets thus have virtually identical pyroxene/grossular ratios (Py<sub>79</sub>Gr<sub>21</sub> and Py<sub>81</sub>Gr<sub>19</sub>, respectively), but almandine contents spanning the majority of compositions found in Earth's upper mantle (Fig. 1). On the basis of calculated pyroxene and garnet stoichiometries, we find no evidence for significant amounts of Fe<sup>3+</sup> in our crystals. *f*O<sub>2</sub> calculations after Holloway et al. (1992) confirm that most of the Fe<sup>3+</sup> remaining in the starting material ( $\pm 95\%$ ) was reduced to Fe<sup>2+</sup> by the presence of the graphite capsule. Pyroxene crystals were generally too small for SIMS analyses, only one crystal in experiment 18 could be analysed for trace elements.

Calculated partition coefficients ( $D^{\text{Grt/Melt}}$  and  $D^{\text{Px/Melt}}$ ) are presented in Table 4. All trace ele-

Table 3  
Major and trace element composition of experimental products

	16 (Grt: Py <sub>72</sub> Gr <sub>19</sub> Alm <sub>9</sub> )						18 (Grt: Py <sub>56</sub> Gr <sub>13</sub> Alm <sub>31</sub> )					
	Grt	$\sigma$	Px	$\sigma$	Q	$\sigma$	Grt	$\sigma$	Px	$\sigma$	Q	$\sigma$
FeO	4.84	0.30	3.32	0.09	6.26	0.08	15.80	0.48	14.68	0.30	18.94	0.71
CaO	7.71	0.54	18.80	0.20	14.49	0.47	5.18	0.33	5.80	1.80	9.87	0.54
MgO	20.80	0.52	18.28	0.25	17.14	0.54	15.73	0.43	22.44	1.70	13.19	0.54
Al <sub>2</sub> O <sub>3</sub>	23.49	0.42	8.41	0.62	13.30	0.24	22.49	0.27	4.39	0.32	9.85	0.16
SiO <sub>2</sub>	43.66	0.44	51.45	0.50	47.44	0.06	41.64	0.28	53.03	0.43	47.64	0.43
Total	100.49	0.66	100.26	0.47	98.64	0.15	100.84	0.38	100.33	0.33	99.48	0.37
<i>n</i> (majors)	22		6		3		14		5		14	
Li	1.58	0.76			70.8	3.1	0.37	0.08	20.6		43.3	0.8
K	152	40			11921	1460	2.94	0.95	18.5		2294	162
Sc	20.7	1.5			4.70	0.47	48.3	4.1	6.10		12.9	0.3
Ti	40.5	1.4			193	11	22.8	4.4	8.37		117	1
Sr	21.8	3.9			1204	66	0.71	0.15	8.44		293	8
Y	14.0	0.2			4.80	0.15	25.2	1.3	0.94		10.5	0.1
Zr	14.6	1.8			37.7	1.2	8.50	1.16	0.38		27.8	0.4
Nb	7.66	0.93			442	48	0.48	0.08	0.48		76.3	2.4
La	22.3	1.6			1212	67	0.22	0.02	0.81		74.8	3.3
Pr	3.60	0.42			84.7	2.9	0.65	0.12	0.47		24.9	0.9
Sm	7.04	0.57			30.0	0.9	3.96	0.50	0.66		19.1	0.3
Tb	11.1	0.5			9.59	0.12	13.5	0.7	0.90		12.9	0.4
Er	14.9	0.3			6.21	0.26	31.3	2.0	0.94		10.6	0.2
Yb	15.7	1.0			3.06	0.09	38.6	3.6	0.95		8.86	0.32
Lu	26.2	1.9			4.16	0.11	33.7	4.3	0.66		6.80	0.02
Hf	12.9	1.8			33.6	1.5	9.23	1.19	0.51		23.2	1.0
Ta	7.85	1.13			321	27	0.59	0.12	0.28		58.7	5.1
Re	1.28	0.44			0.74	0.27	2.63	3.12	0.61		1.47	0.21
Th	13.7	1.9			525	34	0.86	0.14	1.15		114	3
U	6.81	1.85			178	16	0.94	0.12	0.37		38.8	0.5
<i>n</i> (traces)	3				5		3		1		3	

Major elements in weight percent, trace elements in parts per million. Grt = garnet, Px = pyroxene, Q = quench phase.

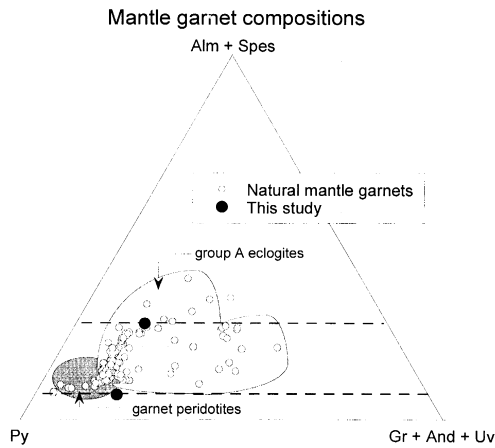


Fig. 1. Iron contents of garnets produced in this study span a significant part of the range found in mantle garnets. Mantle garnet data from compilations of Mottana (1986) and the authors. Light grey field: garnet compositions in group A eclogites. Dark grey field: garnet compositions in fertile garnet peridotites.

ments reported here are incompatible in pigeonite, and values of  $D^{\text{Px}/\text{Melt}}$  are in good agreement with opx–melt REE partitioning data from Salters and Longhi (1999). The highest  $D$  values are 0.48 for lithium, 0.47 for scandium, and 0.42 for rhenium.  $D^{\text{Px}/\text{Melt}}$  for the HREE is around 0.1, which is about 10 times higher than  $D$  values for the LREE. U is slightly less compatible than Th, although the difference is small. These data could have use in future trace element models of melting in the lunar/Martian mantle. In agreement with previous experimental data (Righter and Hauri, 1998), Re is compatible in garnet, although the error in  $D_{\text{Re}}$  is large. This might be caused by the presence of a Re alloy phase in crystals and/or melt. Although no alloy blebs were observed during electron probe analysis, it is impossible to mass-balance Re in our experiments, and the blebs might have been too small to be detected. Li is very incompatible, as previously observed (Van Westrenen et al., 1999). As expected, U is more compatible than Th in garnet. The HREE are compatible in garnet, with maximum  $D$  values for Lu up to 6.3. The LREE are two orders of magnitude less compatible than the HREE.

In Fig. 2a,  $D^{\text{Grt}/\text{Melt}}$  are compared with our previous results on Fe-free garnets at  $P$  and  $T$  conditions virtually identical to those applied here (Van Westre-

nen et al., 1999). Patterns are very similar. Incompatible elements (i.e. those with  $D^{\text{Grt}/\text{Melt}} < 1$ ) are generally slightly more incompatible in Fe-bearing systems, while compatible elements (with  $D^{\text{Grt}/\text{Melt}} > 1$ ) are at the high end of the CMAS range. Fractionations between some geochemically important element pairs (U–Th, Zr–Hf, Nb–Ta) show significant variation with garnet composition. This is illustrated in Fig. 2b, which shows data on  $D_{\text{Zr}}/D_{\text{Hf}}$  and  $D_{\text{U}}/D_{\text{Th}}$  from this study and Van Westrenen et al. (1999). Garnets with either high (Py + Alm), such as those found in fertile peridotites, or very high Gr contents, have  $D_{\text{Zr}}/D_{\text{Hf}}$  smaller than one. However, garnets with more intermediate compositions, closer to those found in eclogites, have  $D_{\text{Zr}}/D_{\text{Hf}}$  larger than one. These same garnets have significantly lower  $D_{\text{U}}/D_{\text{Th}}$  than found in more peridotitic garnets rich in (Py + Alm). Fig. 2b clearly illustrates the impor-

Table 4  
Garnet–melt and pyroxene–melt partition coefficients

Element	16		18			
	$D^{\text{Grt}/\text{melt}}$	$\sigma$	$D^{\text{Grt}/\text{melt}}$	$\sigma$	$D^{\text{Px}/\text{melt}}$	$\sigma$
Fe	0.77	0.05	0.83	0.04	0.78	0.03
Ca	0.53	0.04	0.52	0.04	0.59	0.19
Mg	1.21	0.05	1.19	0.06	1.70	0.15
Al	1.77	0.05	2.28	0.05	0.45	0.03
Si	0.92	0.01	0.87	0.01	1.11	0.01
Li	0.022	0.011	0.0084	0.0018	0.48	0.01
K	0.013	0.004	0.0013	0.0004	0.0081	0.00057
Sc	4.41	0.54	3.75	0.33	0.47	0.0092
Ti	0.2	0.014	0.19	0.04	0.071	0.00037
Sr	0.02	0.0034	0.0024	0.0005	0.029	0.00081
Y	2.91	0.10	2.40	0.13	0.090	0.0011
Zr	0.39	0.05	0.31	0.04	0.014	0.00019
Nb	0.017	0.003	0.0062	0.0011	0.0062	0.00020
La	0.018	0.002	0.0029	0.0003	0.011	0.00048
Pr	0.043	0.005	0.026	0.005	0.019	0.00071
Sm	0.23	0.02	0.21	0.03	0.034	0.00046
Tb	1.16	0.05	1.04	0.07	0.070	0.0022
Er	2.40	0.11	2.97	0.19	0.089	0.0017
Yb	5.14	0.36	4.36	0.43	0.11	0.0039
Lu	6.29	0.48	4.95	0.64	0.097	0.00031
Hf	0.38	0.06	0.40	0.05	0.022	0.0010
Ta	0.024	0.004	0.010	0.0022	0.0047	0.00041
Re	1.73	0.87	1.79	2.14	0.42	0.060
Th	0.026	0.004	0.0075	0.0013	0.010	0.00029
U	0.038	0.011	0.024	0.003	0.0096	0.00011

All values calculated using Table 3.

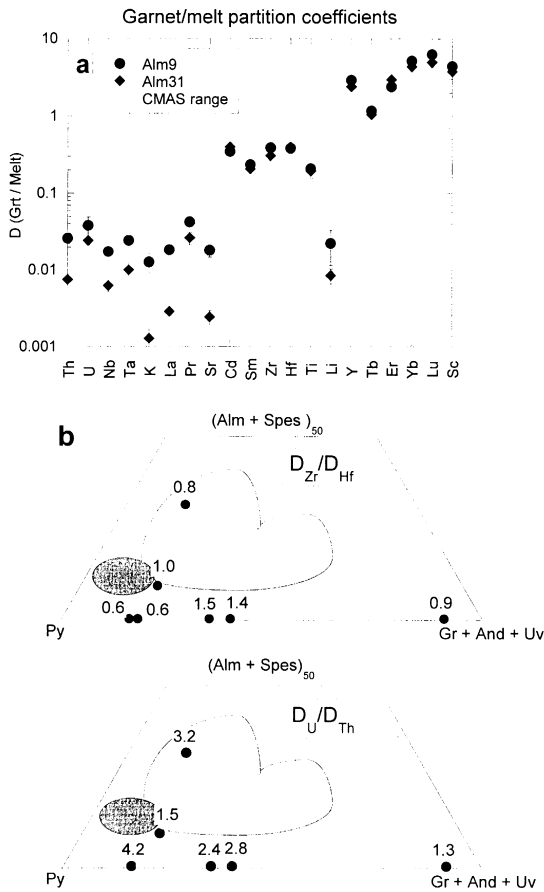


Fig. 2. (a) Spidergram comparing  $D^{\text{Grt}/\text{Melt}}$  from this study with the range observed for experiments at similar  $P$  and  $T$  conditions in CMAS (Van Westrenen et al., 1999). Error bars are  $1\sigma$ . (b) Variation of garnet-melt  $D_{\text{Zr}}/D_{\text{Hf}}$  and  $D_{\text{U}}/D_{\text{Th}}$  with garnet composition. Data taken from Table 4 and from Van Westrenen et al. (1999). Symbols show garnet compositions, with calculated fractionations given adjacent to each point.  $1\sigma$  errors on all values are  $\pm 10\%$  relative. Light and dark grey fields encompass garnet compositions from group A eclogites and fertile garnet peridotites, respectively.

tance of taking into account crystal-chemical variations when studying fractionation of element pairs during mantle melting involving garnet.

Plots of  $\log(D^{\text{Grt}/\text{Melt}})$  versus ionic radius  $r$  ("Onuma diagrams") for divalent and trivalent trace elements entering the garnet X-site are given in Fig. 3. The plots show a near-parabolic dependence of  $D$  on ionic radius, as observed first by Onuma et al. (1968) and borne out by later analyses on a wide

range of mineral–melt pairs (e.g. Jensen, 1973; Blundy and Wood, 1991; Liu et al., 1992; Beattie, 1994; LaTourrette et al., 1995; Brenan et al., 1995; Wood and Blundy, 1997; Van Westrenen et al., 1999). This near-parabolic dependence was quantified by fitting the data to Eq. (1). Fitted curves are shown in Fig. 3, and best-fit parameters given in Table 5. Fitted curves agree very well with the data, with the exception of La and Pr in experiment 16 (Fig. 3a), which have higher  $D^{\text{Grt}/\text{Melt}}$  than expected from the fitted curve. This could be caused by the relatively small amount of melt (21%, Table 2) in this experiment, leading to an increase by a factor of

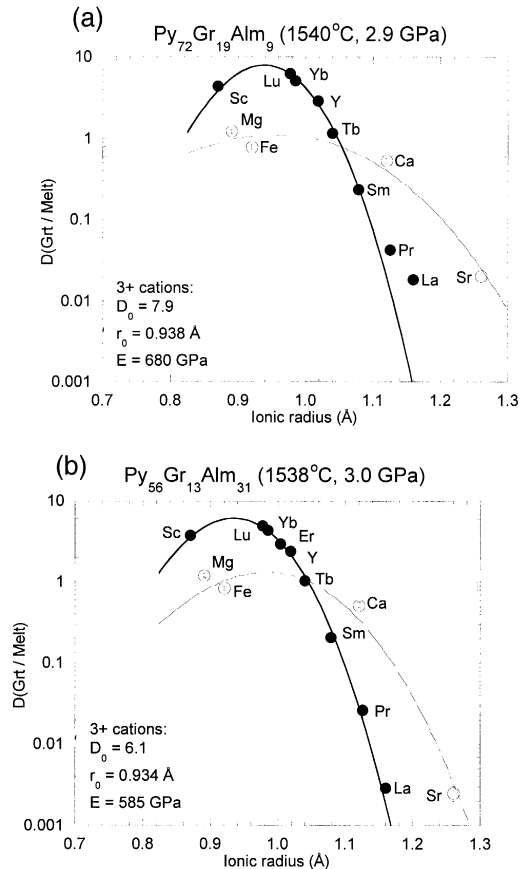


Fig. 3. Onuma diagrams for experiments 16 (a) and 18 (b), showing  $D^{\text{Grt}/\text{Melt}}$  for divalent and trivalent cations entering the garnet X-site (symbols) together with nonlinear least-squares fits to Eq. (1) (curves). Error bars (shown if bigger than symbols) are  $1\sigma$ . Ionic radii taken from Shannon (1976).

Table 5

Results of fitting partitioning data for divalent and trivalent cations entering the garnet X-site to Eq. (1)

	Py <sub>72</sub> Gr <sub>19</sub> Alm <sub>9</sub>		Py <sub>56</sub> Gr <sub>13</sub> Alm <sub>31</sub>	
	Value	$\sigma$	Value	$\sigma$
$r_0(2+)$	0.964	0.027	0.983	0.006
$D_0(2+)$	1.0	0.2	1.3	0.1
$E_X(2+)$	156	56	265	18
$r_0(3+)$	0.938	0.002	0.934	0.001
$D_0(3+)$	7.9	0.4	6.1	0.3
$E_X(3+)$	680	50	585	35

$r_0$  in Å,  $E_X$  in GPa.

6 in Pr and La in the course of the experiment, or by a very small amount of glass contamination (on the order of 1%) during SIMS analysis of the garnet crystals. Neither of these scenarios would influence the  $D$ 's of the other REE significantly. In this case, we believe the fitted curve gives a better description of the true  $D$  than the measured values.

As in the Fe-free experiments,  $r_0(3+) < r_0(2+)$ , and  $E_X(2+) < E_X(3+)$ . Values of  $E_X$  are slightly higher than those for CMAS garnets, while  $r_0$  values are slightly smaller than or equal to lowest values for Fe-free experiments. This qualitatively explains the incompatible element trends in Fig. 2a: the smaller  $r_0$  and the higher  $E$ , the more incompatible (misfit) elements like U, Th, K in the X-site (and by analogy Hf, Zr in the Y-site) become. Higher values for compatible elements are reflected in high values of  $D_0$  ( $\sim 7.9$  and  $\sim 6.1$  for experiments 16 and 18, compared with a maximum of  $\sim 4.8$  in CMAS at similar  $T$  and  $P$ ). As shown by Wood and Blundy (1997),  $D_0$  is partly determined by melt composition, but a quantification of this effect is beyond the scope of this paper. With regards to the pigeonite–melt data, we confine ourselves to remarking that predicted values of  $r_0(3+)$  and  $E_X(3+)$  for the pyroxene in experiment 18 for elements entering the M2 site (0.964 Å and 283 GPa, using Wood and Blundy, 1997) are in excellent agreement with fitted values ( $r_0(3+) = 0.964 \pm 0.02$  Å;  $E_X(3+) = 269 \pm 92$  GPa). It therefore appears the clinopyroxene–melt model of Wood and Blundy (1997) can also be used to predict systematics of pigeonite–melt partitioning.

## 4. Discussion

Because the garnets produced in this study have a near-constant Py–Gr ratio (Py<sub>80±1</sub>Gr<sub>20±1</sub>) but very different almandine contents, the effect of almandine content on partitioning can be quantified. This is illustrated in Fig. 4, which depicts  $r_0(3+)$  as a function of almandine content. The value for iron-free garnets with composition Py<sub>80</sub>Gr<sub>20</sub> is derived from our previous work in CMAS (Van Westrenen et al., 1999). Fig. 4 shows a small dependence of  $r_0(3+)$  on almandine content in our experiments. Our extrapolated value for pure (Mg and Ca-free) almandine, 0.916 Å, compares favourably with the radius of the almandine X-site measured at ambient conditions ( $\sim 0.915$  Å, from the compilation of Smyth and Bish, 1988). Combined with our previous work under similar  $P$ – $T$  conditions we derive the following predictive equation for  $r_0(3+)$  in FCMAS garnets at 3.0 GPa and  $\sim 1540^\circ\text{C}$ :

$$r_0(3+) [\text{Å}] = 0.930 X_{\text{Py}} + 0.993 X_{\text{Gr}} + 0.916 X_{\text{Alm}} \quad (2)$$

Eq. (2) shows that the  $r_0(3+)$  we predict for pure almandine (0.915 Å) is lower than that for pure pyrope (0.930 Å), even though crystallographic data

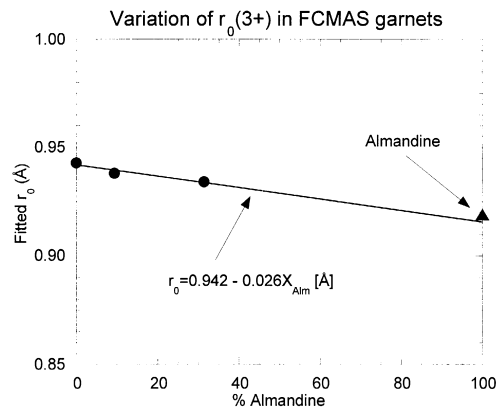


Fig. 4. Variation of  $r_0(3+)$  in FCMAS garnets as a function of garnet iron content, at constant Py–Gr ratio (Py<sub>80</sub>Gr<sub>20</sub>). The value of  $r_0(3+)$  for iron-free garnet (Py<sub>80</sub>Gr<sub>20</sub>Alm<sub>0</sub>) is taken from Van Westrenen et al. (1999). Crystallographically determined X-site radius for almandine (triangle) from Smyth and Bish (1988). For explanation see text.

indicate that at ambient conditions the X-site is smaller in pyrope than in almandine. This might reflect small differences between garnet crystal structure for  $P$ – $T$  versus ambient conditions, or alternatively it might be a result of the large and/or linear extrapolation from our experimental data (maximum of 31% almandine) to pure end-member almandine. We do believe Eq. (1) is valid up to at least  $X_{\text{Alm}} = 0.5$ , a range that incorporates the great majority of natural mantle garnet samples (e.g. Fig. 1).

Almandine, grossular and pyrope components together typically make up 70 to 90% of mantle garnets.  $\text{Fe}^{3+}$  and  $\text{Mn}^{2+}$  contents are usually low (< 1 wt.% of the corresponding oxides  $\text{Fe}_2\text{O}_3$  and  $\text{MnO}$ ), as are  $\text{Cr}^{3+}$  contents in undepleted mantle rocks. Chromium is however an important component of mantle garnets in rocks that have gone through one or more stages of partial melting. In such depleted mantle rocks,  $\text{Cr}_2\text{O}_3$  is present in the garnets at levels of 5–12 wt.%. To take some account of the (generally small) influence of these components on  $r_0(3+)$  we added terms to Eq. (2) for end-members spessartine, andradite, and uvarovite, using as an estimate the radius of the relevant X-sites derived from crystallographic data at ambient conditions (Smyth and Bish, 1988):

$$r_0(3+) [\text{\AA}] = 0.930X_{\text{Py}} + 0.993X_{\text{Gr}} + 0.916X_{\text{Alm}} + 0.946X_{\text{Spes}} + 1.05(X_{\text{And}} + X_{\text{Uv}}) \quad (3)$$

The numerical values in these last two added terms should be adjusted in the future when experiments aimed specifically at the influence of these components are performed. They do however give an indication of the probable influence of these components on  $r_0(3+)$ : large amounts of Cr and trivalent iron will tend to increase  $r_0(3+)$ , while spessartine has less influence as its X-site is intermediate in size between those of almandine, grossular and pyrope. To take into account the fact that garnet X-sites decrease in size with increasing pressure, we added a small pressure correction term to Eq. (3),

$$r_0(3+) [\text{\AA}] = 0.930X_{\text{Py}} + 0.993X_{\text{Gr}} + 0.916X_{\text{Alm}} + 0.946X_{\text{Spes}} + 1.05(X_{\text{And}} + X_{\text{Uv}}) - 0.005(P [\text{GPa}] - 3.0) \quad (4)$$

The value of  $-0.005 \text{\AA}/\text{GPa}$  is in close agreement with observations on the compressibility of the pyrope X-site ( $-0.0045 \text{\AA}/\text{GPa}$ ; Zhang et al., 1998). To assess the accuracy of Eq. (4), comparisons between predicted and observed values of  $r_0(3+)$  at different pressures and temperatures are needed. The existing data sets on natural garnet phenocryst or megacryst–matrix pairs (Irving and Frey, 1978; Liu et al., 1992; Schnetzler and Philpotts, 1970; Sisson and Bacon, 1992) are unsuitable since  $P$  and  $T$  are not sufficiently well-constrained. Of 48 experiments found in the literature, only eight are suitable: (a) They do not contain appreciable amounts of water (< 3 wt.%) — Van Westrenen et al. (2000) have shown that large variations in the melt coordination environment of trace elements, such as might result from the presence of significant amounts of water, could influence values of  $r_0$ . (b) They contain more than three of the relevant trace elements, so that meaningful fits to Eq. (1) can be made. (c) They include data for scandium. Exclusion of Sc from garnet–melt partitioning experiments is a major problem when trying to rationalise garnet–melt partitioning data, as illustrated in Fig. 5a for an experiment from Salters and Longhi (1999). Weighted nonlinear least squares regression of their data to Eq. (1) leads to fitted values of  $r_0(3+)$ ,  $D_0(3+)$  and  $E_X(3+)$  which are physically unrealistic (0.76  $\text{\AA}$ , 60, and 214 GPa respectively, all with large error bars; compare this with fitted values in Table 2). Without Sc it is impossible to constrain the left limb of fitted curves (i.e. for radii smaller than  $r_0$ ). Sc-free experiments therefore cannot be used for deriving  $P$  and  $T$  influence of  $r_0(3+)$ .

We thus compared predicted and fitted values of  $r_0(3+)$  for three experiments from Barth et al. (1997), the experiment described by Hauri et al. (1994), and two each from Rocholl et al. (1996) and Withers (1997). Resulting agreement between predicted and fitted  $r_0(3+)$  is good (Fig. 6): predictions are accurate to within 0.005  $\text{\AA}$ , a value within the error on the fitted values and smaller than the difference in radius between adjacent REE. We did not observe any dependence of  $r_0$  on  $T$ , that is, regressions including a  $T$  term returned a value that is zero within uncertainty.

The next requirement for a fully predictive model for garnet–melt partitioning is a relation between

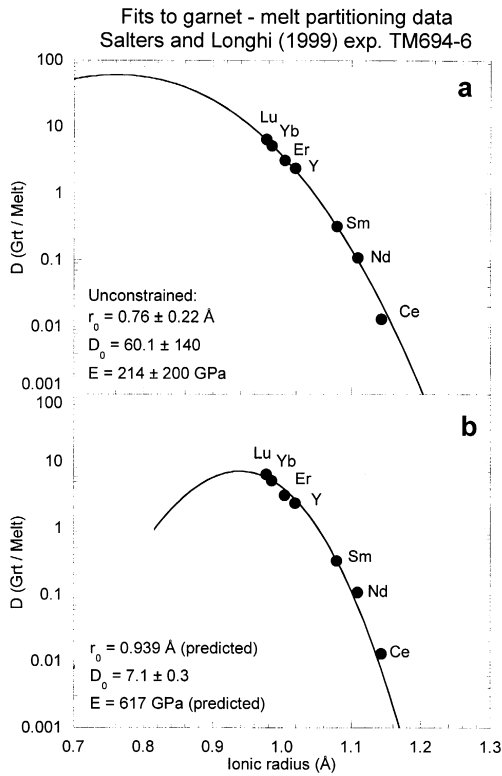


Fig. 5. Fits of Eq. (1) to data from a garnet-melt partitioning experiment by Salters and Longhi (1999) [ $P = 2.8$  GPa,  $T = 1537^\circ\text{C}$ ]. (a) Unconstrained least-squares fit. (b) Fit incorporating predicted values of  $r_0(3+)$  and  $E_X(3+)$ , using Eqs. (4) and (7).

some garnet property or properties and the apparent Young's modulus  $E_X$  (or bulk modulus  $K$ , which is equivalent to  $2/3E$ ) obtained from fitting data to Eq. (1). It has long been known there is a close link between the bulk modulus of a substance and the nature and arrangement of its constituent atoms (e.g. Bridgman, 1923). In the 70s, several workers derived empirical relations between  $K$ , composition and structure, for both bulk materials and their constituent polyhedra. For oxides and silicates, Hazen and Finger (1979) proposed an empirical relation between the volume of a cation-oxygen polyhedron (taken to be  $d^3$ , where  $d = r_0 + 1.38$  Å, the radius of  $\text{O}^{2-}$ ), the charge  $Z_c$  of the cation occupying the polyhedron, and the bulk modulus  $K$  of the corresponding cation oxide:

$$K = 750(\pm 20) \frac{Z_c}{d^3} \quad (5)$$

Eq. (5) shows that both a small polyhedral volume and a high cation charge can result in a high value of  $K$ . Eq. (5) shows some promise for application to mineral-melt partitioning models: analyses of partitioning data for series of trace elements with identical charge  $Z_c$ , using Eq. (1), provide fitted values for both  $K$  (i.e.  $2/3 E$ ) and  $d$  (i.e.  $r_{\text{Oxygen}} + r_0$ ). Wood and Blundy (1997) tested whether  $K$  and  $d$  derived from partitioning data agree with Eq. (5), and found reasonable agreement for  $Z_c = 1, 2$  and  $3$  for clinopyroxene- and plagioclase-melt pairs. Were Eq. (5) to hold for garnet-melt partitioning data, it could be used in conjunction with Eq. (4) to predict  $E_X(3+)$  as a function of garnet composition and  $P$ . However, Fig. 7 shows that Eq. (5) cannot be used to predict  $K_X(3+)$  (and hence  $E_X(3+)$ ) for  $3+$  elements entering the garnet X-site: fitted values of  $K_X(3+)$ , for the experiments in this study, our previous study (Van Westrenen et al., 1999), and the eight Sc-bearing experiments shown in Fig. 6, are markedly higher (by up to a factor of 2) than predicted with Eq. (5), especially at high values of  $Z_c/d^3$  (i.e. at small X-site volumes). These high  $E$  values are difficult to reconcile with any model of garnet elasticity. Recently, computer simulations of

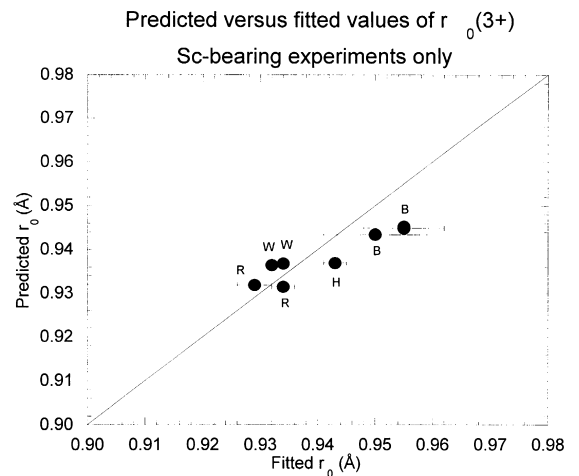


Fig. 6. Comparison between fitted values of  $r_0(3+)$  and values predicted using Eq. (4), for all existing Sc-bearing,  $\text{H}_2\text{O}$ -poor experimental garnet-melt partitioning data. R = Rocholl et al. (1996),  $P = 5$  GPa; B = Barth et al. (1997),  $P = 1.8$  GPa; H = Hauri et al. (1994),  $P = 2.5$  GPa; W = Withers (1997),  $P = 3.0$  GPa. Error bars in fitted values are  $1\sigma$ .

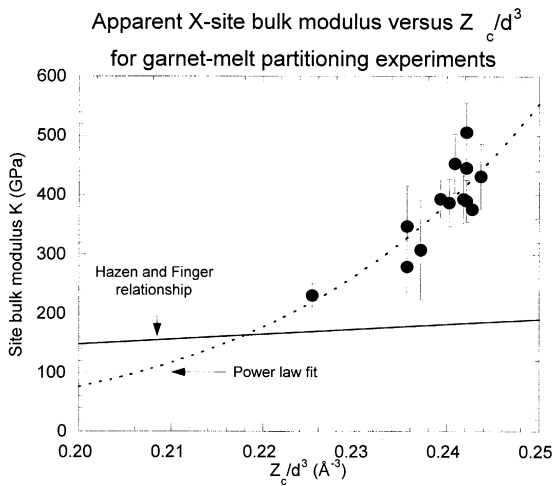


Fig. 7. Bulk modulus  $K$  versus cation charge ( $Z_c$ ) divided by cation–oxygen distance cubed ( $d^3$ ) derived from garnet–melt partitioning data. Error bars are  $1\sigma$ . The large discrepancy between partitioning data and relation found by Hazen and Finger (1979) (Eq. (5)) for polyhedra in oxides is apparent. Dotted line is power law fit to the data (Eq. (6)).

trace element incorporation into garnets (Van Westrenen et al., 2000) have shown that the coordination number of both major and trace elements in the melt can influence the apparent site modulus  $E$  derived from partitioning data. Specifically, the lower the coordination number of a trace element in a melt, the higher the apparent  $E$  derived from partitioning studies between garnet and that melt. Clearly, more work needs to be done to find a satisfactory theoretical model for the variation seen in Fig. 7. In the absence of such a model, we have to take a more empirical approach. The garnet–melt data appear to show a power law dependence of  $K$  on  $V$  ( $=d^3$ , see the dotted line in Fig. 7). Such a dependence is in accordance with Anderson (1972), who shows that  $KV^y = \text{constant}$  for iso-structural groups of elements, oxides, halides, and sulphides. For oxide data,  $y$  is close to 1, in agreement with Eq. (5). Fitting the partitioning data to a power law (Fig. 7) gives

$$\begin{aligned} K_X(3+) [\text{GPa}] &= 2.3 \times 10^{12} (V [\text{\AA}^3])^{-8.9} \\ &= 2.3 \times 10^{12} (1.38 + r_0(3+) [\text{\AA}])^{-26.7} \end{aligned} \quad (6)$$

The best-fit value of  $y$  (8.9) is outside the range found by Anderson (1972) for oxides, halides, elements, and sulphides ( $1 < y < 5$ ), another indication that a factor other than garnet elasticity must influence  $K$  derived from partitioning studies. For trivalent cations entering the garnet X-site, the apparent site Young's modulus can be estimated by assuming a Poisson's ratio of 0.25:

$$\begin{aligned} E_X(3+) [\text{GPa}] &= 1.5K_X(3+) \\ &= 3.5 \times 10^{12} (1.38 + r_0(3+) [\text{\AA}])^{-26.7} \end{aligned} \quad (7)$$

with a standard deviation of around 30 GPa.

Imposing predicted  $r_0(3+)$  and  $E_X(3+)$  onto experiments without Sc increases the plausibility of fits dramatically, shown in Fig. 5b for an experiment of Salters and Longhi (1999). It is important to note that the data in this figure were not used as input for the model, and the quality of the fit is a true reflection of predictive capabilities. Eqs. (4) and (7) work equally well for all ‘anhydrous’ experiments not used as input in the model, and also seem applicable to experiments containing larger ( $> 3$  wt.%) amounts of water (e.g. Green et al., 2000). The latter observation suggests that, contrary to the concerns expressed earlier, water does not have a significant bearing on  $r_0$ . This emphasises once again the overriding influence of crystal properties on partitioning behaviour. Overall, partition coefficients for the HREE, Y and Sc are reproduced to within  $\sim 10\%$  relative in the 48 experimental data sets; the error can be larger (up to  $\sim 40\%$ ) for the LREE, primarily because partition coefficients are low ( $< 0.1$ ). Of course,  $D_0$  is still a fitted parameter at this stage, so that the true accuracy of our model might be somewhat overestimated. A full evaluation of the accuracy of our models must await development of predictions for  $D_0(3+)$ . It is clear, however, that the equations derived above can be used to predict with reasonable accuracy garnet–melt partition coefficients under a wide range of  $P$ ,  $T$  and  $X$  conditions. At this stage, knowledge of just one  $D_{\text{REE/Y/Sc}}$  is sufficient to predict  $D_{\text{Grt/Melt}}$  for all other REE, Sc and Y to within 10–40% relative. Moreover, even in the absence of such knowledge, important information about relative values of partition coefficients can be obtained. As an illustration

of this last point, we discuss some implications of our model for mantle melting in the presence of garnet.

## 5. Implications for mantle melting

There are several garnet reservoirs in the Earth's upper mantle, e.g. undepleted and depleted garnet peridotites, group-A eclogites, garnet pyroxenite veins and so on. These reservoirs are present at a wide range of  $P$  and  $T$  conditions, and garnet major element compositions generally also differ between and within reservoirs (e.g. Fig. 1). It should be clear from the foregoing discussion that variations in  $P$ ,  $T$  and  $X$  all influence partition coefficients. Fig. 2b illustrates this point for some important trace element pairs (Zr–Hf and U–Th). Our data show that at the same  $P$  and  $T$ , partial melting of eclogites may lead to fractionation of these pairs that is at least different from, and plausibly opposite to, that expected by partial melting of fertile garnet-bearing peridotites.

For the REE, Y, and Sc we now have a means of quantitatively assessing the influence  $X$  has on  $D^{\text{Grt}/\text{Melt}}$ . To this end we collected major element data from the literature on a wide range of mantle garnets, and used Eq. (3) to predict values of  $r_0(3+)$  (i.e., to a first approximation we neglected the small influence of pressure on  $r_0(3+)$ ). We predict that  $r_0(3+)$  during partial melting of fertile garnet peridotite is almost constant at  $0.939 \pm 0.005 \text{ \AA}$  (number of garnets  $n = 17$ ). Garnets in pyroxenite veins impose values of  $r_0(3+)$  in the range  $0.932\text{--}0.943 \text{ \AA}$  ( $n = 26$ ). Depleted garnet reservoirs show slightly higher values:  $r_0(3+) = 0.953 \pm 0.009 \text{ \AA}$  for garnets in a wide range of depleted mantle xenoliths ( $n = 126$ ) and  $0.941 \pm 0.007 \text{ \AA}$  ( $n = 117$ ) for group A eclogites (garnet major element data from MacKenzie and Canil, 1999; Matsyuk et al., 1998; Robinson and Wood, 1998; Stachel et al., 1998; Brenker and Brey, 1997; Harte and Kirkley, 1997; O'Reilly and Griffin, 1995; Beard et al., 1992; Bell and Rossman, 1992; Sen and Leeman, 1991; Bodinier et al., 1987; Irving, 1974; Boyd and Nixon, 1972). Significantly, these values are all considerably smaller than the radius of the smallest REE, Lu ( $r = 0.977 \text{ \AA}$ ). As a consequence, during mantle

melting in the presence of virtually any natural mantle garnet,  $D_{\text{Lu}}$  will always be larger than  $D^{\text{Grt}/\text{Melt}}$  of any other REE, as well as Sc and Y. One implication of our prediction is that the flat HREE patterns found in the experiments of Hauri et al. (1994), with  $D_{\text{Er}} > D_{\text{Yb}} > D_{\text{Lu}}$ , are probably erroneous. Another implication, stemming from the link between  $r_0(3+)$  and  $E$  in Eq. (7), is that  $E_X(3+)$  varies from  $\sim 520$  GPa for garnets found in depleted mantle xenoliths to  $\sim 620$  GPa for garnets in undepleted peridotites. Both lower values of  $r_0(3+)$  and higher values of  $E_X(3+)$  in garnets from fertile mantle will cause a larger fractionation between adjacent REE. For instance, at  $1500^\circ\text{C}$  and 3 GPa, an undepleted garnet ( $r_0(3+) = 0.939 \text{ \AA}$ ,  $E_X(3+) = 620$  GPa) is predicted to have a  $D_{\text{Sm}}^{\text{Grt}/\text{Melt}}/D_{\text{Nd}}^{\text{Grt}/\text{Melt}}$  of 5.1, while we predict a value of 3.4 for a depleted garnet ( $r_0(3+) = 0.953 \text{ \AA}$ ,  $E_X(3+) = 520$  GPa) under the same  $P$  and  $T$  conditions.

## 6. Conclusions

We have presented new experimental garnet–melt partitioning data in the simple system FCMAS. Interpretation of our data using the model of Blundy and Wood (1994) yields equations for the variation of  $r_0(3+)$  and  $E_X(3+)$  as a function of garnet composition and pressure. It is important to realise that these equations could not have been derived from the existing garnet–melt database alone, largely because of (a) the scarcity of Sc partitioning data with which to constrain the size of the garnet X-site, and (b) the interdependence of composition,  $P$  and  $T$  in experiments on natural compositions. To disentangle these interdependencies, experiments in simple systems, at constant  $P$  and  $T$  conditions, are essential. Although the experiments discussed in this paper are not *directly* applicable to natural garnet–melt systems because of their particular combination of  $P$ ,  $T$  and  $X$  conditions, at least as much information is derived from them as from experiments aimed at mimicking as closely as possible “natural” conditions.

Although our model is not yet fully predictive (absolute values of  $D^{\text{Grt}/\text{Melt}}$  cannot be predicted unless  $D^{\text{Grt}/\text{Melt}}$  for one isovalent cation entering the same garnet lattice is known), the equations (Eqs. (4) and (7)) provide valuable insights into the variation

of garnet–melt partition coefficients during mantle melting in the presence of garnet. What is required for a fully predictive model now is knowledge of the variation of  $D_0$  as a function of  $P$ ,  $T$  and melt composition.

### Acknowledgements

Stuart Kearns, John Craven, and Richard Hinton are thanked for their essential help during EMPA and SIMS analysis. This work also benefited greatly from the technical expertise of Fred Wheeler, Mike Dury and Prof. J.F. Hasselbaink. James Brenan and Reidar Trønnes are thanked for their thoughtful reviews. The editorial efforts of Håkon Austrheim are much appreciated. WvW acknowledges the EU Fourth Framework Programme (contract ERBFMBICT 971991) for financial support. JDB acknowledges a research fellowship from the Royal Society.

### References

- Anderson, O.L., 1972. Patterns in elastic constants of minerals important to geophysics. In: Robertson, E.C. (Ed.), *The Nature of the Solid Earth*. McGraw-Hill, pp. 575–613.
- Barth, M.G., Foley, S.F., Horn, I., 1997. Experimental trace element partitioning in tonalitic systems. *LPI Contrib.* 921, 18.
- Beard, B.L., Medaris, L.G., Johnson, C.M., Brückner, H.K., Misar, Z., 1992. Petrogenesis of Variscan high-temperature group-A eclogites from the Moldanubian zone of the Bohemian Massif, Czechoslovakia. *Contrib. Mineral. Petrol.* 111, 468–483.
- Beattie, P., 1993. Uranium–thorium disequilibria and partitioning on melting of garnet peridotite. *Nature* 363, 63–65.
- Beattie, P., 1994. Systematics and energetics of trace-element partitioning between olivine and silicate melts: implications for the nature of mineral/melt partitioning. *Chem. Geol.* 117, 57–71.
- Bell, D.R., Rossman, G.R., 1992. The distribution of hydroxyl in garnets from the subcontinental mantle of Southern Africa. *Contrib. Mineral. Petrol.* 111, 161–178.
- Blichert-Toft, J., Albarède, F., Kornprobst, J., 1999. Lu–Hf isotope systematics of garnet pyroxenites from Beni Bousera, Morocco: implications for basalt origin. *Science* 283, 1303–1306.
- Blundy, J.D., Wood, B.J., 1991. Crystal-chemical controls on the partitioning of Sr and Ba between plagioclase feldspar, silicate melts and hydrothermal solutions. *Geochim. Cosmochim. Acta* 55, 193–209.
- Blundy, J.D., Wood, B.J., 1994. Prediction of crystal–melt partition coefficients from elastic moduli. *Nature* 372, 452–454.
- Blundy, J.D., Robinson, J.A.C., Wood, B.J., 1998. Heavy REE are compatible in clinopyroxene on the spinel lherzolite solidus. *Earth Planet. Sci. Lett.* 160, 493–504.
- Bodinier, J.L., Guiraud, M., Fabriès, J., Dostal, J., Dupuy, C., 1987. Petrogenesis of layered pyroxenites from the Lherz, Freychinède and Prades ultramafic bodies (Ariège, French Pyrénées). *Geochim. Cosmochim. Acta* 51, 279–290.
- Bourdon, B., Zindler, A., Elliott, T., Langmuir, C.H., 1996. Constraints on mantle melting at mid-ocean ridges from global  $^{238}\text{U}$ – $^{230}\text{Th}$  disequilibrium data. *Nature* 384, 231–235.
- Boyd, F.R., Nixon, P.H., 1972. Ultramafic nodules from the Thaba Putsoa kimberlite pipe. *Carnegie Inst. Washington, Year Book* 71, 362–373.
- Brenan, J.M., Shaw, H.F., Ryerson, F.J., Phinney, D.L., 1995. Experimental determination of trace-element partitioning between pargasite and a synthetic hydrous andesitic melt. *Earth Planet. Sci. Lett.* 135, 1–11.
- Brenker, F.E., Brey, G.P., 1997. Reconstruction of the exhumation path of the Alpe Arami garnet–peridotite body from depths exceeding 160 km. *J. Metamorph. Geol.* 15, 581–592.
- Bridgman, P.W., 1923. The compressibility of thirty metals as a function of pressure and temperature. *Proc. Am. Acad. Arts Sci.* 58, 165–242.
- Green, T.H., Blundy, J.D., Adam, J., Yaxley, G.M., 2000. SIMS determination of trace element partition coefficients between garnet, clinopyroxene and hydrous basaltic liquids at 2–7.5 GPa and 1080–1200°C. This volume.
- Harte, B., Kirkley, M.B., 1997. Partitioning of trace elements between clinopyroxene and garnet: data from mantle eclogites. *Chem. Geol.* 136, 1–24.
- Hauri, E.H., Wagner, T.P., Grove, T.L., 1994. Experimental and natural partitioning of Th, U, Pb and other trace elements between garnet, clinopyroxene and basaltic melts. *Chem. Geol.* 117, 149–166.
- Hazen, R.M., Finger, L.W., 1979. Bulk modulus–volume relationship for cation–anion polyhedra. *J. Geophys. Res.* 84, 6723–6728.
- Hirschmann, M.M., Stolper, E.M., 1996. A possible role for garnet pyroxenite in the origin of the “garnet signature” in MORB. *Contrib. Mineral. Petrol.* 124, 185–208.
- Holloway, J.R., Pan, V., Gudmundsson, H., 1992. High-pressure fluid-absent melting experiments in the presence of graphite: oxygen fugacity, ferric/ferrous ratio and dissolved  $\text{CO}_2$ . *Eur. J. Mineral.* 4, 105–114.
- Irving, A.J., 1974. Geochemical and high pressure experimental studies of garnet pyroxenite and pyroxene granulite xenoliths from the Delegate basaltic pipes. *Aust. J. Petrol.* 15, 1–40.
- Irving, A.J., Frey, F.A., 1978. Distribution of trace elements between garnet megacrysts and host volcanic liquids of kimberlitic to rhyolitic composition. *Geochim. Cosmochim. Acta* 42, 771–787.
- Jensen, B.B., 1973. Patterns of trace element partitioning. *Geochim. Cosmochim. Acta* 37, 2227–2242.
- LaTourrette, T.Z., Kennedy, A.K., Wasserburg, G.J., 1993. Thorium–uranium fractionation by garnet: evidence for a deep source and rapid rise of oceanic basalts. *Science* 261, 739–742.
- LaTourrette, T.Z., Hervig, R.L., Holloway, J.R., 1995. Trace

- element partitioning between amphibole, phlogopite, and basanite melt. *Earth Planet. Sci. Lett.* 135, 13–30.
- Liu, C.-Q., Masuda, A., Shimizu, H., Takahashi, K., Xie, G.-H., 1992. Evidence for pressure dependence of the peak position in the REE mineral/melt partition patterns of clinopyroxene. *Geochim. Cosmochim. Acta* 56, 1523–1530.
- Longhi, J., 1992. Experimental petrology and petrogenesis of mare volcanics. *Geochim. Cosmochim. Acta* 56, 2235–2251.
- MacKenzie, J.M., Canil, D., 1999. Composition and thermal evolution of cratonic mantle beneath the central Archean Slave Province, NWT, Canada. *Contrib. Mineral. Petrol.* 134, 313–324.
- Matsyuk, S.S., Langer, K., Hosch, A., 1998. Hydroxyl defects in garnets from mantle xenoliths in kimberlites of the Siberian Platform. *Contrib. Mineral. Petrol.* 132, 163–179.
- Mottana, A., 1986. Crystal-chemical evaluation of garnet and omphacite microprobe analyses: its bearing on the classification of eclogites. *Lithos* 19, 171–186.
- Onuma, N., Higuchi, H., Wakita, H., Nagasawa, H., 1968. Trace element partition between two pyroxenes and the host lava. *Earth Planet. Sci. Lett.* 5, 47–51.
- O'Reilly, S.Y., Griffin, W.L., 1995. Trace-element partitioning between garnet and clinopyroxene in mantle-derived pyroxenites and eclogites:  $P$ - $T$ - $X$  controls. *Chem. Geol.* 121, 105–130.
- Perkins, D. III, Holland, T.J.B., Newton, R.C., 1981. The  $Al_2O_3$  contents of enstatite in equilibrium with garnet in the system  $MgO$ - $Al_2O_3$ - $SiO_2$  at 15–40 kbar and 900–1600°C. *Contrib. Mineral. Petrol.* 78, 99–109.
- Righter, K., Hauri, E.H., 1998. Compatibility of rhenium in garnet during mantle melting and magma genesis. *Science* 280, 1737–1741.
- Robinson, J.A.C., Wood, B.J., 1998. The depth of the garnet/spinel transition in fractionally melting peridotite. *Earth Planet. Sci. Lett.* 164, 277–284.
- Rocholl, A., Ludwig, T., Altherr, R., Meyer, H.-P., Brey, G., Velz, S., Seck, H.-A., Bulatov, V., 1996. Experimental partitioning of trace elements between clinopyroxene, garnet and basanitic melts studied by ion microprobe. *J. Conf. Abs.* 1, 517–518.
- Salter, V.J.M., 1996. The generation of mid-ocean ridge basalts from the Hf and Nd isotope perspective. *Earth Planet. Sci. Lett.* 141, 109–123.
- Salter, V.J.M., Longhi, J., 1999. Trace element partitioning during the initial stages of melting beneath mid-ocean ridges. *Earth Planet. Sci. Lett.* 166, 15–30.
- Schnetzer, C.C., Philpotts, J.A., 1970. Partition coefficients of rare-earth elements between igneous matrix material and rock-forming mineral phenocrysts — II. *Geochim. Cosmochim. Acta* 34, 331–340.
- Sen, G., Leeman, W.P., 1991. Iron-rich lherzolitic xenoliths from Oahu: origin and implications for Hawaiian magma sources. *Earth Planet. Sci. Lett.* 102, 45–57.
- Shannon, R.D., 1976. Revised effective ionic radii and systematic studies of interatomic distances in halides and chalcogenides. *Acta Cryst. A* 32, 751–767.
- Shen, Y., Forsyth, D.W., 1995. Geochemical constraints on the initial and final depth of melting beneath mid-ocean ridges. *J. Geophys. Res.* 100, 2211–2237.
- Sisson, T.W., Bacon, C.R., 1992. Garnet/high silica rhyolite trace element partition coefficients measured by ion microprobe. *Geochim. Cosmochim. Acta* 56, 2133–2136.
- Smyth, J.R., Bish, D.L., 1988. *Crystal Structures and Cation Sites of the Rock-Forming Minerals*. Allen and Unwin.
- Stachel, T., Viljoen, K.S., Brey, G., Harris, J.W., 1998. Metasomatic processes in lherzolitic and harzburgitic domains of diamondiferous mantle: REE in garnets from xenoliths and inclusions in diamonds. *Earth Planet. Sci. Lett.* 159, 1–12.
- Van Westrenen, W., Blundy, J.D., Wood, B.J., 1999. Crystal-chemical controls on trace element partitioning between garnet and anhydrous silicate melt. *Am. Mineral.* 84, 838–847.
- Van Westrenen, W., Allan, N.L., Blundy, J.D., Purton, J.A., Wood, B.J., 2000. Atomistic simulation of trace element incorporation into garnets — comparison with experimental garnet–melt partitioning data. *Geochim. Cosmochim. Acta* 64, 1629–1639.
- Withers, A.C., 1997. Water in the mantle. Unpublished Doctor of Philosophy thesis, University of Bristol, United Kingdom.
- Wood, B.J., Blundy, J.D., 1997. A predictive model for rare earth element partitioning between clinopyroxene and anhydrous silicate melt. *Contrib. Mineral. Petrol.* 129, 166–181.
- Wood, B.J., Blundy, J.D., Robinson, J.A.C., 1999. The role of clinopyroxene in generating U-series disequilibrium during mantle melting. *Geochim. Cosmochim. Acta* 63, 1613–1620.
- Zhang, L., Ahsbahs, H., Kutoglu, A., 1998. Hydrostatic compression and crystal structure of pyrope up to 33 GPa. *Phys. Chem. Miner.* 25, 301–307.